H. Böhm, M. Braun-Unkhoff, Numerical study on the effect of oxygenated blending compounds on soot formation, Combust. Flame 153 (2008) 84-96.

The original publication is available at www.elsevier.com

http://dx.doi.org/10.1016/j.combustflame.2008.01.002

Numerical study of the effect of oxygenated blending compounds on soot formation in shock tubes

H. Böhm[1], M. Braun-Unkhoff[2]
[1] *Physikalische Chemie I, Universität Bielefeld, Germany*
[2] *Deutsches Zentrum für Luft- und Raumfahrt e.V., Stuttgart, Germany*

Abstract
This numerical study deals with the influence of blends on the amount of soot formed in shock tubes, which were simulated by assuming a homogeneous plug flow reactor model. For this purpose, first, the reaction model used here was validated against experimental results previously obtained in the literature. Then, the soot volume fractions of various mixtures of methyl *tert*-butyl ether (MTBE)–benzene, isobutene–benzene, methanol–benzene, and ethanol–benzene diluted in argon were simulated and compared to the results of benzene–argon pyrolysis at 1721 K and 5.4 MPa. For MTBE, isobutene, methanol, and ethanol, small amounts of additives to benzene–argon mixtures promoted soot formation, for the shock tube model assumed, while higher concentrations of these additives led to smaller soot volume fractions in comparison to pure benzene–argon pyrolysis. The most significant soot promotion effect was found for the additives MTBE and isobutene. The channel for MTBE decomposition producing isobutene and methanol is very effective at temperatures beyond 1200 K. Thus, both MTBE–benzene and isobutene–benzene mixtures diluted in argon showed rather similar behavior in regard to soot formation. Special emphasis was directed toward the causes for the concentration-dependent influence of the blends on the amount of soot formed. Aromatic hydrocarbons and acetylene were identified as key gas-phase species that determine the trends in the formation of soot of various mixtures. From reaction flux analysis for phenanthrene, it was deduced that the combinative routes including phenyl species play a major role in forming PAHs, especially at early reaction times. It is found that the additives play an important role in providing material to grow side chains, such as by reaction channels including phenylacetylene or benzyl, which are confirmed to form aromatic hydrocarbons and thus to influence the amount of soot formed, particularly when the concentrations of the blends are increased.

Keywords: Oxygenated blending compounds; PAH; Soot

1. Introduction

In the past decade, the formation of polycyclic aromatic hydrocarbons (PAHs) and soot particles has become one of the central themes of research activities in the area of combustion and pyrolysis of hydrocarbon fuels. Numerous experimental, theoretical, and computational investigations are devoted to the study of physical and chemical properties of soot formation [1–8]. However, modeling the complete soot formation process still remains a challenging task; in particular, mechanistic understanding and reliable description of the formation of small aromatic structures are of fundamental interest and are critical for meaningful soot modeling with the aim of reducing respective emissions from combustion processes.

The interest in this subject results mostly from environmental concerns with pollutant emission from combustion devices. Many airborne species of health concern are generated by combustion processes such as transportation, power generation, and waste incineration. In particular, some aromatics and PAHs are toxic and subject to environmental regulations. Epidemiologists have provided strong indication of an association of cancer and cardiovascular disease with atmospheric aerosols [9–11]. Polycyclic aromatic hydrocarbons are associated with aerosol particles of different sizes [11,12], and evidence of mutagenic or tumorigenic effects of many of them has been identified [11,13]. In addition to their direct healthhazardous effects, strong evidence for the key role of PAHs in the formation of soot has been accumulated in recent years [2,3,14,15]. Fine particulates are responsible for heart and lung diseases [16,17] and may contribute to global warming [18].

Aromatics may be emitted in significant amounts by ground vehicles and airplanes resulting from the combustion of practical fuels such as kerosene; they may be important constituents of the fuel itself. For example, gasoline consists of up to 32% aromatics [19], and kerosene is a complex mixture of alkanes, mono- and polycyclic aromatics, and cycloalkanes or naphthenes [20]. The assembly of benzene as the first aromatic ring from its precursor molecules is commonly considered as the first step toward PAH formation and growth [2,21–23].

The limited resources of fossil fuels such as oil and natural gas require new concepts, in particular for transportation fuels and for electric power generation. Over the past years, alternative and renewable energy resources have become increasingly important as they have contributed to reducing the dependency on fossil fuels and to decreasing CO2 and thus greenhouse gas emission, which contribute to climate change [24]. Low-quality feedstock such as biomass, in particular, has a large potential for power generation, for instance, in gas turbines via gasification process or in an IGCC (integrated gasification combined cycle) plant [25–29].

Quite recently, the European Commission made proposals for a new energy policy for Europe [30]. These included a renewable energy roadmap proposing (i) a binding 20% target for the overall share of renewable energy in 2020 as well as (ii) a binding 10% target for the share of biofuels in petrol and diesel in each member state in 2020, to be accompanied by the introduction of a sustainability scheme for biofuels. Concerning liquid transportation fuel, biomass provides the only renewable alternative; the two most common types of biofuels are ethanol and biodiesel [31,32]. They can be blended with or directly substitute for gasoline and diesel, respectively. Currently, ethanol is widely used as a fuel additive or even as a fuel to cut down a vehicle's carbon monoxide and other smog-causing emissions, e.g., E10 (10% ethanol and 90% gasoline blend) and E85 (85% ethanol and 15% gasoline blend). The latter can be used as a substitute for gasoline in flexible-fuel vehicles that have been modified to use this biofuel and that run on mixtures of gasoline and up to 85% ethanol. Biodiesel can be used as an additive to reduce vehicle emissions (typically 20%) or in its pure form as a renewable alternative fuel for diesel engines. However, it should be remarked that soot derived from the combustion of soybean-oil-derived biodiesel fuel has been reported to be about five times more reactive than soot obtained

from combustion of a Fischer–Tropsch (FT) diesel fuel [33]. Most reformulated gasoline components produced from biomass are pollution-reducing fuel additives, such as methyl tertiary butyl ether (MTBE)—which may come from isobutylene and biomethanol—and ethyl tertiary butyl ether (ETBE).

Since society is shifting to the burning of biomassbased fuels, the effect of oxygen-containing fuels on the byproducts of combustion is of increasing interest. From previous studies [34–42], it is known that several alcohol and ether blends are able to suppress engine "knock" and to reduce the amount of polyaromatic hydrocarbons (PAHs) as well as soot formed during the process of combustion. However, none of these studies focused on systematic investigation of a possible change of soot-suppressing into soot-promoting effects of oxygenated blends dependent on their concentration, especially for carbon-rich reaction mixtures, such as for shock tube pyrolysis of aromatic fuels.

Aromatic fuels desirable in gasoline to increase the octane number are known to soot more than aliphatic ones. In the present work, benzene was chosen as a representative aromatic fuel for the numerical investigation of various blend ratios of the oxygen-containing aliphatic fuels MTBE, methanol, and ethanol as well as of isobutene, which is formed by MTBE decomposition, in argon-diluted mixtures in shock tubes. This study was encouraged by the results of Knorre et al. [43], who found higher soot yields for several benzene–aliphatic mixtures than for the pure fuels in shock tube experiments. Thus, in the present study on shock tubes, similar behavior of mixtures of oxygenated fuels, isobutene and benzene is looked for, namely, a soot-suppressing effect of the additives methanol, ethanol, and MTBE that possibly changes into a soot-promoting effect in dependence on the blend ratios.

2. Modeling and experimental results

The reaction mechanism used for the modeling study contained 185 species and 718 reactions. The core of the reaction mechanism was gathered from the work of Böhm et al. [44] and was used previously for modeling species profiles and soot particles in laminar premixed flames and shock tube studies [4–8]. MTBE chemistry as proposed and validated by Böhm et al. [36] and by Curran et al. [45] was incorporated into the mechanism. Reactions for ethanol and isobutene (i-C_4H_8) formation and consumption relied also on [45]. The rate coefficients for phenanthrene formation via benzyl recombination and 1,2-diphenylethane and stilbene formation followed the work of Colket and Seery [46] and the estimates of Hebgen [47]. The reactions modified or extended in comparison to [44] are given in Table 1.

Computer simulations of the shock tube studies were performed with the SENKIN kinetic program of the CHEMKIN II package [51]. The program input includes forward reaction rates and thermodynamic polynomials for all of the participating species in addition to temperature, pressure, and concentrations of the reactants.

For the soot model, the method of moments as described in [52] was used including improvements of the initial model, namely the use of detailed PAH chemistry instead of the lumping procedure for PAHs. Furthermore, all PAHs with more than 200 amu were allowed to coagulate [44]. Surface growth of acetylene and PAHs was taken into account. In addition, the sticking coefficient was calculated based on [21], the particle coagulation was assumed to be pressuredependent, and OH radicals and O2 molecules were regarded as responsible for the oxidation of the soot particles [53].

From the literature, three different shock tube experiments from two different groups were used for validation [35,54]. The shock tube studies considered were first a methanol–benzene–argon mixture at a pressure of 0.25 MPa, with mole fractions of x(Ar) = 0.99378, $x(C_6H_6) = x(CH_3OH)$ = 0.00311, and an ethanol–benzene–argon mixture at 0.22 MPa with x(Ar) = 0.99378, $x(C_6H_6) = x(C_2H_5OH)$ = 0.00311 as experimentally investigated by Frenklach et al. [35] within the temperature range between 1600 and 2400 K. To minimize the effect of varying temperature on the results, for the calculations the same initial temperature of T = 1721 K was chosen as for the following set of experiments, that is, as for the pyrolysis of benzene–argon mixtures [54].

The influence of temperature on soot formation is given by the well-known bell-shaped behavior of soot leading to maximum soot yields at around 1800 to 1850 K for benzene pyrolysis (see, for example, in [43]). A temperature of 1721 K, that is, roughly 100 K below maximum soot production, was chosen for the calculation, since our reaction model was verified successfully for this reaction condition several times (see, e.g., [44]).

The pyrolysis behavior of these benzene–argon mixtures without (experimental data from [54]) as described in [44] and with small amounts of aliphatics was calculated under initial conditions of 5.4 MPa and 1721 K. The aliphatics chosen were MTBE, methanol, ethanol, and isobutene. The last is an important decomposition product of MTBE. For details of the various mixture compositions, see Table 2.

3. Results and discussion

3.1. Validation of the mechanism

To validate the reaction mechanism used for the predictions, calculations were performed and compared to experimental results previously obtained in the literature. Fig. 1 displays the profiles of the simulated soot volume fraction for methanol–benzene– argon pyrolysis and for ethanol–benzene–argon pyrolysis. For the experimental results, only one single point for each mixture is available from [35]. The calculations show an overprediction of the soot volume fraction for both mixtures at a reaction time of 1.0 ms by a factor approximately of 2.7.

A further validation of the modeling and the experimentally obtained soot volume profiles [44] is given in Fig. 2 for benzene–argon pyrolysis without any additive at 5.4 MPa and an initial temperature of 1721 K. It can be seen that the agreement between the simulations and the experiments is

reasonable, concerning the absolute values as well as the shape of the curves. However, the calculations show a slight underprediction of the soot volume fractions, especially at short reaction times. Further checks of (parts of) the reaction model used here were carried out (see [4–8]) and gave satisfactory agreement between experiments and calculations.

3.2. Soot formation in benzene–argon pyrolysis with blending compounds

After this satisfactory predictive capability check of the gas phase and soot chemistry used, the remainder of this investigation is focused on effects of varying additive concentrations on the soot volume fraction of benzene–argon pyrolysis. First, small blend ratios were chosen with 10% replacement of benzene by the additive MTBE, methanol, ethanol, or isobutene (Mix2). Isobutene was also chosen as an additive because of its important role during MTBE decomposition (as discussed below in more detail). The resulting calculated profiles of the soot volume fractions are depicted in Fig. 3. From these calculations it is obvious that all additives investigated here do not suppress soot formation but promote it, especially at short reaction times. The efficiency of the promoting effect is given by the ranking MTBE > isobutene > ethanol ≈ methanol.

In exploring the other extreme, Fig. 4 displays the calculated soot volume fractions fv of aliphatic–benzene–argon pyrolysis for a replacement of 70% of benzene by oxygenated aliphatics or isobutene (Mix7). In this case, the soot volume fraction of the aliphatic–benzene–argon pyrolysis is decreased compared to that of the pure benzene–argon pyrolysis. The minimum reduction of soot is caused by methanol addition, followed by that of ethanol, MTBE, and isobutene.

For a systematic investigation of the concentration-dependent effects of the four additives on soot formed during benzene–argon pyrolysis, Fig. 5 is presented. It shows the soot volume fraction fv as a function of the percentage of benzene replaced by the additives (Mix0 to Mix8) at the reaction time t of 2.0ms. From the pure benzene–argon pyrolysis to the mixtures with the highest additive concentrations (Mix8), the soot volume fraction is seen to decrease. It reaches a maximum between 5% and 20% of replacement of benzene and then decreases. For MTBE and isobutene additives, this maximum becomes much more significant than in those curves achieved for the added alcohols ethanol and methanol, where the maximum is not very clearly indicated. More pronounced maxima are obtained in the case of constant carbon density calculations. For example, for 5% ethanol replacement of benzene in benzene/argon pyrolysis at constant carbon density and otherwise identical reaction conditions as given for Mix1, the soot volume fraction fv is increased to about 1.0×10^{-5} cm^3 per cm^3 exhaust and thus reaches a clear maximum value.

Consequently, the calculations predict a promoting effect on soot formation for benzene–argon pyrolysis in the case of very small blend ratios of oxygenated additives or isobutene, changing into a soot-suppressing effect at higher concentrations of these additives. This behavior found for oxygenated aliphatics and isobutene seems to be qualitatively similar to those of acetylene blend to

benzene–argon pyrolysis. In this reaction system, the soot yields for several acetylene–benzene–argon mixtures were reported to be higher than those for the pure fuels [43]. The interesting result is worth inspecting more closely, in particular with regard to selected species, namely H, H_2, C_2H_2, and PAHs, which are known to play an important role during the soot formation process [55]. To examine whether these species reflect the same dependence on the blend ratio as the soot volume fraction, Figs. 6–8 are plotted.

The availability of radicals—in the pyrolysis systems investigated here, mainly the presence of H atoms—is postulated to be a rate-determining step during the growth of PAH and soot [21] by producing radicals via

$$\text{soot}+\text{H}\rightarrow\text{soot-radical}+\text{H}_2, \tag{61}$$

whereas the resulting soot radicals can add acetylene molecules or PAHs from the gas phase leading to the process of soot mass growth. Therefore, in Fig. 6, the ratios of the mole fraction of H to that of H_2 versus the percentage of benzene replaced by the additives MTBE, isobutene, methanol, and ethanol are displayed at the reaction time t of 2.0 ms. For all four curves, the ratio of the mole fraction of H to the one of H_2 exhibits a monotonic decrease as the amounts of additive is increased. In contrast, the soot volume fraction curves in Fig. 5 show a maximum as a function of the blend ratio and thus look totally different from those in Fig. 6.

In Fig. 7, the mole fraction x of acetylene, a species of relevance for soot mass growth, versus the percentage of benzene replaced by the additives MTBE, isobutene, ethanol, and methanol is plotted at the reaction time t of 2.0 ms. The highest acetylene fractions are predicted for MTBE, followed by those of isobutene, ethanol, and methanol. This is in accord with the soot volume fractions shown in Fig. 5, where the highest values are found for MTBE, followed by those of isobutene, ethanol, and methanol. However in Fig. 7, for MTBE and isobutene, the mole fractions of acetylene are enhanced with increasing concentration of the blending compound. Against that, in Fig. 5, the soot volume fractions fv are decreased at high concentrations of the blends. For methanol and ethanol, the curves of the mole fraction x of acetylene versus the percentage of benzene replacement by additives lead through a maximum. For these two alcohols, a maximum of the soot volume fraction curves is found also in Fig. 5, but the shape of this smooth maximum is rather different from the corresponding acetylene curve in Fig. 7.

Besides hydrogen and acetylene, the PAHs are proposed as important key species during the formation process of soot, especially concerning their leading role for soot precursor formation. Thus, as for hydrogen and acetylene, the dependence of the PAH concentration on the concentration of the blending compound is inspected in the following. For this, the sums of the mole fraction x of all aromatic hydrocarbons with a mass of more than 178 amu are plotted versus the percentage of replacement of benzene by the additives MTBE, isobutene, methanol, and ethanol at the reaction time

t of 2.0 ms in Fig. 8. The highest PAH mole fractions are found for MTBE; the lowest are those for methanol. The curves of the sum of mole fraction *x* of the PAHs decline monotonically as the concentration of the blends isobutene, methanol, and ethanol is increased, as to be expected. Only one PAH mole fraction curve, namely that for MTBE as an additive, peaks smoothly, at approximately 5% replacement of benzene, followed by a monotonic decrease. In comparing the curves in Fig. 5, that is, the behavior of the soot volume fraction *f*v versus the blending compound concentration, and those in Fig. 8, that is, the PAH mole fraction versus blending compound concentration, the following has to be stated: Neither the observed increase of the soot volume fraction *f*v nor the position of the maximum of the curves in Fig. 5, is in accordance with the plots in Fig. 8. Only the declining part of the curves of the soot volume fraction for the four additives is mirrored by the decreasing mole fractions of the PAH versus the percentage of replacement of benzene.

Since none of the species' concentrations considered so far, that is, neither the concentrations of H, H_2, or acetylene, nor that of the PAHs, were able to correlate the observed change of a soot-promoting with a soot-suppressing effect of the oxygenated blending compounds studied, a better correlation is looked for in the following. For this, the acetylene mole fractions multiplied by the sum of PAH mole fractions versus the percentage of benzene replacement by additives at the reaction time *t* of 2.0 ms are illustrated in Fig. 9. The highest product values are found for MTBE, followed by isobutene, ethanol, and methanol. The same trend was calculated for the soot volume fraction of the four additives in Fig. 5. The curves of $x(\text{PAH}) \times x(C_2H_2)$ in Fig. 9 peak between 10% and 20% replacement of benzene, as also predicted for the corresponding curves of the soot volume fraction in Fig. 5. Furthermore, the calculated maximum value and the shape of the curves $x(\text{PAH}) \times x(C_2H_2)$ are in satisfactory qualitative agreement with the curves of the soot volume fractions shown in Fig. 5. Thus, the product of the mole fraction of acetylene and of the PAHs seems to reasonably reflect the change of the soot-promoting into the soot-suppressing effect of oxygenated blending compounds as a function of their concentration in benzene–argon pyrolysis.

Finally, in comparing Fig. 7 and Fig. 8, it can be seen that high concentrations of blending compounds favor the formation of acetylene at the cost of PAH formation, whereas MTBE and isobutene addition causes higher acetylene concentrations than ethanol or methanol blending. At the same time, the amount of the soot volume fraction *f*v displayed in Fig. 5 is reduced. Thus, at low ratios of PAH to acetylene concentration, *f*v seems to be most sensitive to the availability of PAHs, not to that of acetylene. Against that, at low concentrations of the blending compounds in benzene–argon pyrolysis, and thus at a high ratio of the PAH to acetylene concentration, *f*v seems to be promoted by an increase of the acetylene concentration. These results indicate that there is a specific acetylene-to-PAH concentration for each additive where the soot volume fraction *f*v production is greatest. At the same time, interestingly, the calculated soot volume fractions in the present study do not show a significant dependence on the H and/or the H_2 concentration.

Additional calculations carried out at T = 1821 K according to experimental conditions from [43] indicate that the observations made in the present work, namely the increase of soot volume fractions for benzene pyrolysis by small amounts of additive, hold at least for MTBE and isobutene. At the same time, the maximum soot volume produced is shifted to slightly smaller amounts of replacement of benzene, compared to the results obtained at T = 1721 K.

3.3. Reaction flow analysis

An integral reaction flow analysis was performed as a part of the calculations. As a result, it can be concluded that at high temperatures MTBE is consumed mainly (nearly 100%) by thermal decomposition in all mixtures via

$C_5H_{12}O \rightarrow i\text{-}C_4H_8 + CH_3OH.$ (1)

By this decomposition, the major fractions of $i\text{-}C_4H_8$ and CH_3OH are formed. Isobutene ($i\text{-}C_4H_8$) reacts mainly to the resonance-stabilized radical $i\text{-}C_4H_7$,

$i\text{-}C_4H_8 + H \rightarrow i\text{-}C_4H_7 + H_2,$ (16)

followed by the formation of allene and CH_3 via

$i\text{-}C_4H_7 \rightarrow C_3H_4 + CH_3,$ (23)

whereas C_3H_4 consumption reactions lead to the formation of acetylene, which promotes soot formation. Thus, it becomes clear why in the present study MTBE and isobutene behave rather similarly concerning the soot formation process.

Important sinks for the CH_3OH concentration are the two reactions

$CH_3OH + H \rightarrow CH_2OH + H_2$ (51)

and

$CH_3OH (+M) \rightarrow CH_3 + OH (+M),$ (52)

where (51) attains increasing influence with increasing initial methanol concentrations.

The major part of C_2H_5OH decomposes via two H-abstraction reactions:

$C_2H_5OH + H \rightarrow CH_3CHOH + H_2$ (24)

and

$C_2H_5OH + H \rightarrow CH_2CH_2OH + H_2.$ (25)

In comparison to the H abstraction from the benzene molecule,

$C_6H_6 + H \rightarrow C_6H_5 + H_2$, (53)

the rate coefficients for the H abstraction reactions of the oxygenated molecules and isobutene, that is, for reactions (2), (3), (16), (24), (25), (26), and (51), are increased. Consequently, through the replacement of benzene by the additives, the initiation rates speed up, and the species concentration profiles and soot volume profiles show a steeper incline/decline at early reaction times than for the pure benzene/argon pyrolysis, as can be seen from Figs. 3 and 4.

Relevant formation pathways for aromatic hydrocarbons are discussed for phenanthrene as an example.

In all mixtures, such as for Mix7, shown in Fig. 10, the addition of acetylene to biphenyl is an important formation route:

biphenyl + C_2H_2 →phenanthrene + H_2. (54)

This is especially true for pure benzene–argon pyrolysis, where the rate of production for reaction (54) reaches the highest values. Additionally, combinative growth steps of side chains containing aromatic radicals such as that of phenyl with phenylacetylene and of C_8H_5 isomers with benzene,

$C_8H_6 + C_6H_5 \rightarrow$phenanthrene + H, (55)

$C_8H_5 + C_6H_6 \rightarrow$phenanthrene + H, (56, 57)

contribute significantly to the formation of phenanthrene, especially in mixtures containing low concentrations of additives.

As is to be expected, higher concentrations of the blends in the mixtures cause a decrease of rates of production of the aromatic compounds such as phenanthrene. However, at the same time, an increasing influence of the phenanthrene formation steps via reactions of aromatic hydrocarbons containing CH_3 or CH_2 side chains becomes noticeable, as displayed in Fig. 10. These reaction sequences (44)–(50) lead to 1,2-diphenylethane and furthermore by hydrogen abstraction to stilbene and finally phenanthrene. The growing importance of these formation channels results from increasing CH_3 concentration produced by the blending compounds MTBE, isobutene, methanol, and ethanol, as demonstrated by reactions (23) and (52). Against that, the formation of phenanthrene via cyclopentadienyl and indenyl,

$C_5H_5 + C_9H_7 \rightarrow$phenanthrene + 2H, (58)

is found to be of less importance in the reaction systems investigated here.

Main consumption channels of phenanthrene are the isomerization reaction to form anthracene,

phenanthrene→anthracene, (59)

and the H abstraction reaction,

phenanthrene + H→phenanthryl + H_2. (60)

Thus, in comparison to pure benzene–argon pyrolysis, by adding small amounts of blending components such as MTBE, isobutene, methanol, or ethanol, a higher concentration of aliphatics can be achieved, which are able to serve as side chains and/or "gapfilling species" for aromatic hydrocarbons. By these reaction pathways the latter can form highly condensed ring systems with enhanced stability.

4. Conclusions

The impact of oxygen-containing compounds and isobutene addition on the amount of PAHs and soot produced from benzene–argon mixtures was studied numerically. Higher concentrations of the blends in the mixtures cause an increasing influence of the formation steps to phenanthrene, a representative species for the PAHs, via aromatic hydrocarbons with side chains. Dependent on the amount of the blending compounds MTBE, isobutene, methanol, and ethanol added to benzene diluted in argon in a shock tube at high temperature and high pressure, soot-promoting as well as soot-suppressing effects were predicted. At a high ratio of PAH to acetylene concentration, the soot volume fraction was promoted by an increase of the acetylene concentration. In contrast, at a low ratio of phenanthrene to acetylene concentration, the amount of soot produced seemed to be most sensitive to the availability of PAHs, not to that of acetylene. The product of the mole fraction of acetylene and that of the PAHs reasonably reflected the change of soot-promoting into soot-suppressing effects of oxygenated blending compounds and isobutene. Furthermore, the calculated soot volume fractions were not very sensitive to changes of the H or the H_2 concentrations.

Acknowledgments

The authors thank Dr. H. Jander for her helpful discussions and Kaiyi Huang for assistance in performing the calculations and the figures.

References

[1] H. Bockhorn (Ed.), Detailed Mechanism and Modeling of Soot Particle Formation, Springer-Verlag, Heidelberg, 1994.

[2] H. Richter, J.B. Howard, Prog. Energy Combust. Sci. 26 (2000) 565–608.

[3] M. Frenklach, Phys. Chem. Chem. Phys. 4 (2002) 2028–2037.

[4] M. Braun-Unkhoff, A. Chrysostomou, P. Frank, E. Gutheil, R. Lückerath, W. Stricker, Proc. Combust. Inst. 27 (1998) 329–336.

[5] D. Hu, M. Braun-Unkhoff, P. Frank, Combust. Sci. Technol. 149 (1–6) (1999) 79–94.

[6] D. Hu, M. Braun-Unkhoff, P. Frank, Z. Phys. Chem. 214 (4) (2000) 473–491.

[7] A. Schöbel-Ostertag, M. Braun-Unkhoff, C. Wahl, L. Krebs, Combust. Flame 140 (2005) 359–370.

[8] M. Kamphus, M. Braun-Unkhoff, K. Kohse- Höinghaus, Combust. Flame 152 (2008) 28–59.

[9] D.W. Dockery, C.A. Pope, X. Xu, J.D. Spengler, J.H. Ware, M.E. Fay, B.G. Ferris, F.E. Speizer, N. Engl. J. Med. 329 (1993) 1753–1759.

[10] N. Künzli, R. Kaiser, S. Medina, M. Studnicka, O. Chanel, P. Filliger, M. Herry, F. Horak Jr., V. Puybonnieux-Texier, P. Quénel, J. Schneider, R. Seethaler, J.-C. Vergnaud, H. Sommer, Lancet 356 (2000) 795–801.

[11] C.-E. Boström, P. Gerde, A. Hanberg, B. Jernström, C. Johansson, T. Kyrklund, A. Rannug, M. Törnqvist, K. Victorin, R.Westerholm, Environ. Health Perspect. 110 (2002) 451–489.

[12] J.O. Allen, N.M. Dookeran, K.A. Smith, A.F. Sarofim, K. Taghizadeh, A.L. Lafleur, Environ. Sci. Technol. 30 (1996) 1023–1031.

[13] J.L. Durant, W.F. Busby, A.L. Lafleur, B.W. Penman, C.L. Crespi, Mutation Res. 371 (1996) 123–157.

[14] J.B. Howard, Proc. Combust. Inst. 23 (1990) 1107– 1127.

[15] B.S. Haynes, H.Gg. Wagner, Prog. Energy Combust. Sci. 7 (1981) 229–273.

[16] A. Nel, Science 308 (2005) 804–806.

[17] C.A. Pope III, R.T. Burnett, M.J. Thun, E.E. Calle, D. Krewski, K. Ito, G.D. Thurston, J. Am. Med. Assoc. 287 (2002) 1132–1141.

[18] M.Z. Jacobson, J. Geophys. Res. 107 (2002) 4410– 4431.

[19] R.F. Sawyer, Proc. Combust. Inst. 24 (1992) 1423– 1432.

[20] P. Dagaut, Phys. Chem. Chem. Phys. 4 (2002) 2079– 2094.

[21] M. Frenklach, H. Wang, in: H. Bockhorn (Ed.), Soot Formation in Combustion, Springer-Verlag, Berlin, 1994, pp. 165–192.

[22] N.M. Marinov, W.J. Pitz, C.K. Westbrook, M.J. Castaldi, S.M. Senkan, Combust. Sci. Technol. 116– 117 (1996) 211–287.

[23] J.A. Miller, M.J. Pilling, J. Troe, Proc. Combust. Inst. 30 (2005) 43–88.

[24] R.K. Bhargava, in: Global Energy Market—Past, Present and Future, Proceedings of GT2006, ASME Turbo Expo: GT2006-91322, 2006.

[25] S. Gadde, J. Wu, A. Gulati, G.M. McQuiggan, B. Koestlin, B. Prade, in: Proceedings of GT2006, ASME Turbo Expo: GT2006-90970, 2006.

[26] E.G. Lindfeldt, M.O. Westermark, in: Proceedings of GT2006, ASME Turbo Expo: GT2006-90183, 2006.

[27] F. Delattin, S. Bram, J. De Ruyck, in: Proceedings of GT2006, ASME Turbo Expo: GT2006-90012, 2006.

[28] M. Braun-Unkhoff, Th. Kick, U. Steil, M. Tsurikov, P. Weigand, M. Aigner, in: Proceedings of 14th European Biomass Conference and Exhibition, 2005, pp. 647– 677.

[29] M. Braun-Unkhoff, Th. Kick, P. Frank, M. Aigner, in: Proceedings of GT2007, ASME Turbo Expo: GT2007- 27479, 2007.

[30] http://ec.europa.eu/energy/energy_policy/documents_ en.htm.

[31] E. Forester, D. Assmann, C. Clashausen, in: Proceedings of 14th European Biomass Conference, Paris, France, 2005, pp. 1983–1986.

[32] D. Gielen, F. Unander, in: Proceedings of 14th European Biomass Conference, 2005, pp. 2158–2159.

[33] E. Chapman, A.L. Boehman, in: ACS Symposium: Biofuels for Transportation, Division of Fuel Chemistry, FUEL 14, The 231st National Meeting of the American Chemical Society, 28 March 2006.

[34] R.A. Cox, J.A. Cole, Combust. Flame 60 (1985) 109– 123.

[35] M. Frenklach, T. Yuan, in: H. Grönig (Ed.), Shock Tubes and Waves, Proceedings of the Sixteenth International Symposium on Shock Tubes and Waves, Aachen, 26–31 July 1987, VCH-Verlag, Weinheim, 1988, pp. 487–493.

[36] H. Böhm, F. Baronnet, B. El Kadi, Phys. Chem. Chem. Phys. 2 (2000) 1929–1933.

[37] J. Wu, K.H. Song, T. Litzinger, S.-Y. Lee, R. Santoro, M. Linevsky, M. Colket, D. Liscinsky, Combust. Flame 144 (2006) 675–687.

[38] J. Wu, K.H. Song, T. Litzinger, S.-Y. Lee, R. Santoro, M. Linevsky, Combust. Sci. Technol. 175 (5) (2006) 863–887.

[39] C.-L. Song, W.-M. Zhang, Y.-Q. Pei, G.-L. Fan, G.-P. Xu, Atmos. Environ. 40 (2006) 1957–1970.

[40] C.S. McEnally, L.D. Pfefferle, Proc. Combust. Inst. 31 (2007) 603–610.

[41] N. Miyamoto, H. Ogawa, M.N. Nabi, Int. J. Engine Res. 1 (1) (2000) 71–85.

[42] F.J. Liotta Jr., D.M. Montalvo, SAE Paper 932734, 1993.

[43] V.Gg. Knorre, D. Tanke, T. Thienel, H.Gg. Wagner, Proc. Combust. Inst. 26 (1996) 2303–2310.

[44] H. Böhm, M. Braun-Unkhoff, P. Frank, Prog. Comput. Fluid Dynam. 3 (2–4) (2003) 145–150.

[45] H. Curran, M. Dunphy, J. Simmie, C. Westbrook, W. Pitz, Proc. Combust. Inst. 24 (1992) 769–776.

[46] M.B. Colket, D.J. Seery, Proc. Combust. Inst. 25 (1994) 883–891.

[47] P. Hebgen, Ph.D. thesis, University Darmstadt, Germany, 1996.

[48] J.C. Bauge, F. Battin-Leclerc, F. Baronnet, Int. J. Chem. Kinet. 30 (1998) 632–640.

[49] C.E. Canoa, R.M. Marshall, Int. J. Chem. Kinet. 13 (1981) 303–315.

[50] S.K. Gulati, R.W.Walker, J. Chem. Soc. Faraday Trans. II 84 (1988) 401–411.

[51] R.J. Kee, F.M. Rupley, J.A. Miller, CHEMKIN: The Chemkin Thermodynamic Database, Report SAND87- 8215, Sandia National Laboratories, Livermore, CA, 1987.

[52] H. Wang, M. Frenklach, Combust. Flame 110 (1997) 173–221.

[53] A. Kazakov, H. Wang, M. Frenklach, Combust. Flame 110 (1995) 111–120.

[54] D. Tanke, Ph.D. thesis, University Göttingen, Germany, 1995.

[55] I. Glassman, Proc. Combust. Inst. 22 (1988) 295–311.

Table 1
Reactions for MTBE, isobutene, ethanol, 1,2-diphenylethane, and stilbene

No. reaction	A (cm^3 mol s)	n	E_a (J/mol)	Reference
Reactions for MTBE				
1. $C_5H_{12}O \leftrightarrow iC_4H_8 + CH_3OH$	4.00E+13	0.0	2.47E+05	[36]
2. $C_5H_{12}O + H \leftrightarrow C_5H_{11}O\hat{}1 + H_2$	8.32E+07	2.0	3.22E+04	[45]
3. $C_5H_{12}O + H \leftrightarrow C_5H_{11}O\hat{}2 + H_2$	1.32E+07	2.0	2.09E+04	[45]
4. $C_5H_{12}O + O \leftrightarrow C_5H_{11}O\hat{}1 + OH$	6.61E+06	2.4	2.30E+04	[45]
5. $C_5H_{12}O + O \leftrightarrow C_5H_{11}O\hat{}2 + OH$	4.17E+13	0.0	2.18E+04	[45]
6. $C_5H_{12}O + OH \leftrightarrow C_5H_{11}O\hat{}2 + H_2O$	3.16E+12	0.0	3.09E+03	[45]
7. $C_5H_{12}O + OH \leftrightarrow C_5H_{11}O\hat{}1 + H_2O$	1.55E+10	0.97	6.66E+03	[45]
8. $C_5H_{12}O + CH_3 \leftrightarrow C_5H_{11}O\hat{}2 + CH_4$	6.03E+11	0.0	3.98E+04	[45]
9. $C_5H_{12}O + CH_3 \leftrightarrow C_5H_{11}O\hat{}1 + CH_4$	1.95E+12	0.0	4.86E+04	[45]
10. $C_5H_{12}O + HO_2 \leftrightarrow C_5H_{11}O\hat{}2 + H_2O_2$	8.32E+12	0.0	7.41E+04	[45]
11. $C_5H_{12}O + HO_2 \leftrightarrow C_5H_{11}O\hat{}1 + H_2O_2$	1.20E+13	0.0	8.12E+04	[45]
12. $C_5H_{12}O\hat{}1 \leftrightarrow iC_4H_8 + CH_3O$	5.01E+14	0.0	1.04E+05	[36]
13. $C_5H_{11}O\hat{}2 \leftrightarrow tC_4H_9 + CH_2O$	2.51E+14	0.0	8.29E+04	[36]
14. $C_5H_{11}O\hat{}1 \leftrightarrow C_5H_{11}O\hat{}2$	1.58E+12	0.0	6.62E+04	[36]
Reactions for isobutene				
15. $iC_4H_8 + OH \leftrightarrow iC_4H_7 + H_2O$	6.31E+06	2.0	1.25E+03	[45]
16. $iC_4H_8 + H \leftrightarrow iC_4H_7 + H_2$	3.47E+05	2.5	1.04E+04	[45]
17. $iC_4H_8 + CH_3 \leftrightarrow iC_4H_7 + CH_4$	4.46E+00	3.5	1.85E+04	[45]
18. $CH_3 + C_3H_5 \leftrightarrow iC_4H_8$	2.10E+12	0.0	0.0	[48]
19. $iC_4H_8 + O \leftrightarrow iC_4H_7 + OH$	3.47E+11	0.0	2.46E+04	[45]
20. $iC_4H_8 + HO_2 \leftrightarrow iC_4H_7 + H_2O_2$	1.95E+04	2.6	5.82E+04	[45]
21. $tC_4H_9 \leftrightarrow iC_4H_8 + H$	4.70E+14	0.0	1.65E+05	[49]
22. $tC_4H_9 + O_2 \leftrightarrow iC_4H_8 + HO_2$	2.70E+10	0.0	9.10E+03	est. from [50]
23. $iC_4H_7 \leftrightarrow C_3H_4 + CH_3$	1.00E+13	0.0	2.14E+05	[45]
Reactions for ethanol				
24. $C_2H_5OH + H \leftrightarrow CH_3CHOH + H_2$	4.47E+06	2.0	2.09E+04	[45]
25. $C_2H_5OH + H \leftrightarrow CH_2CH_2OH + H_2$	9.12E+06	2.0	3.22E+04	[45]
26. $C_2H_5OH + H \leftrightarrow CH_3CH_2O + H_2$	8.32E+05	2.1	2.04E+04	[45]
27. $C_2H_5OH + O \leftrightarrow CH_3CHOH + OH$	3.09E+13	0.0	2.18E+04	[45]
28. $C_2H_5OH + O \leftrightarrow CH_2CH_2OH + OH$	2.24E+13	0.0	3.22E+04	[45]
29. $C_2H_5OH + O \leftrightarrow CH_3CH_2O + OH$	4.79E+13	0.0	2.87E+04	[45]
30. $C_2H_5OH + OH \leftrightarrow CH_3CHOH + H_2O$	6.76E+07	1.61	1.47E+02	[45]
31. $C_2H_5OH + OH \leftrightarrow CH_2CH_2OH + H_2O$	7.59E+09	0.97	6.64E+03	[45]
32. $C_2H_5OH + OH \leftrightarrow CH_3CH_2O + H_2O$	9.55E+12	0.0	1.36E+04	[45]
33. $C_2H_5OH + CH3 \leftrightarrow CH_3CHOH + CH_4$	1.74E+00	3.46	2.29E+04	[45]
34. $C_2H_5OH + CH3 \leftrightarrow CH_2CH_2OH + CH_4$	3.16E+01	3.17	3.00E+04	[45]
35. $C_2H_5OH + CH3 \leftrightarrow CH_3CH_2O + CH_4$	1.45E+01	3.10	2.90E+04	[45]

36. $C_2H_5OH + HO2 \leftrightarrow CH_3CHOH + H_2O_2$	5.89E+13	0.0	7.41E+04	[45]
37. $C_2H_5OH + HO2 \leftrightarrow CH_2CH_2OH + H_2O_2$	8.32E+12	0.0	8.55E+04	[45]
38. $C_2H_5OH + HO_2 \leftrightarrow CH_3CH_2O + H_2O_2$	9.12E+13	0.0	7.96E+04	[45]
39. $C_2H_5OH \leftrightarrow CH_3 + CH_2OH$	2.51E+16	0.0	8.43E+04	[48]
40. $CH_2CH_2OH \leftrightarrow C_2H_4 + OH$	3.24E+14	−0.24	1.41E+05	[45]
41. $CH_3CHOH + M \leftrightarrow CH_3CHO + H + M$	1.86E+24	−2.5	1.43E+05	[45]
42. $CH_3CHOH + O_2 \leftrightarrow CH_3CHO + HO_2$	4.79E+14	0.0	2.10E+04	[45]
43. $CH_3CH_2O \leftrightarrow CH_3 + CH_2O$	2.09E+12	0.0	9.04E+04	[45]
Reactions for diphenylethane and stilbene				
44. 2 Benzyl→diphenylethane	5.00E+12	0.0	2.00E+03	[46]
45. Diphenylethane→2 benzyl	2.88E+12	0.0	2.78E+05	[46]
46. Diphenylethane + H↔diphenylethyl + H_2	6.65E+06	2.53	5.13E+04	est. from [52]
47. Diphenylethane+OH↔diphenylethyl +H_2O	1.55E+06	2.0	1.80E+03	est. from [52]
48. Diphenylethyl + H↔stilbene + H_2	3.00E+13	0.0	0.0	est. from [52]
49. Diphenylethyl + OH↔stilbene + H_2O	5.00E+12	0.0	0.0	est. from [52]
50. Stilbene↔phenanthrene + H_2	1.00E+08	0.0	1.34E+05	est. from [46]

Note. Rate coefficient $k = A \times T^n \exp(-E_{act}/RT)$.

Table 2
Mole fractions of additive–benzene–argon pyrolysis with the aliphatic fuels MTBE, isobutene, methanol, and ethanol as additives under initial conditions p = 5.4 MPa and T = 1721 K, balanced by 99.8% argon

Mixture	Mole fraction additive x(aliphatic)	Mole fraction benzene x(benzene)
Mix0	0.0	2.0E−03
Mix1	1.0E−04	1.9E−03
Mix2	2.0E−04	1.8E−03
Mix3	3.0E−04	1.7E−03
Mix4	4.0E−04	1.6E−03
Mix5	6.0E−04	1.4E−03
Mix6	1.0E−03	1.0E−03
Mix7	1.4E−03	6.0E−04
Mix8	2.0E−03	0.0

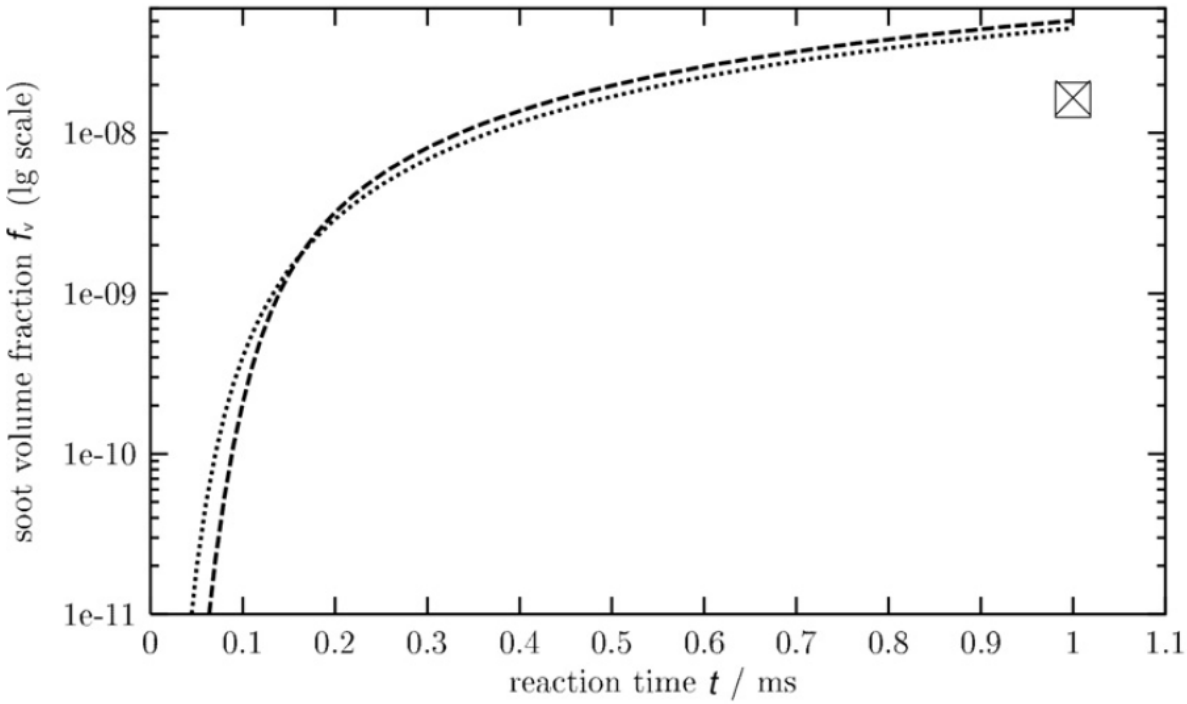

Fig. 1. Calculated (curves) and measured (symbols) [35] soot volume fraction *f*v (logarithmic scale) versus reaction time *t* for (i) methanol–benzene–argon pyrolysis (dotted curve, cross) at initial conditions p = 0.25 MPa, T = 1721 K with mole fractions x(AR) = 0.99378 and $x(C_6H_6) = x(CH_3OH)$ = 0.00311, and (ii) ethanol–benzene–argon pyrolysis (dashed curve, square) at p = 0.22 MPa, T = 1721 K with mole fractions x(AR) = 0.99378 and $x(C_6H_6) = x(CH_3OH)$ = 0.00311.

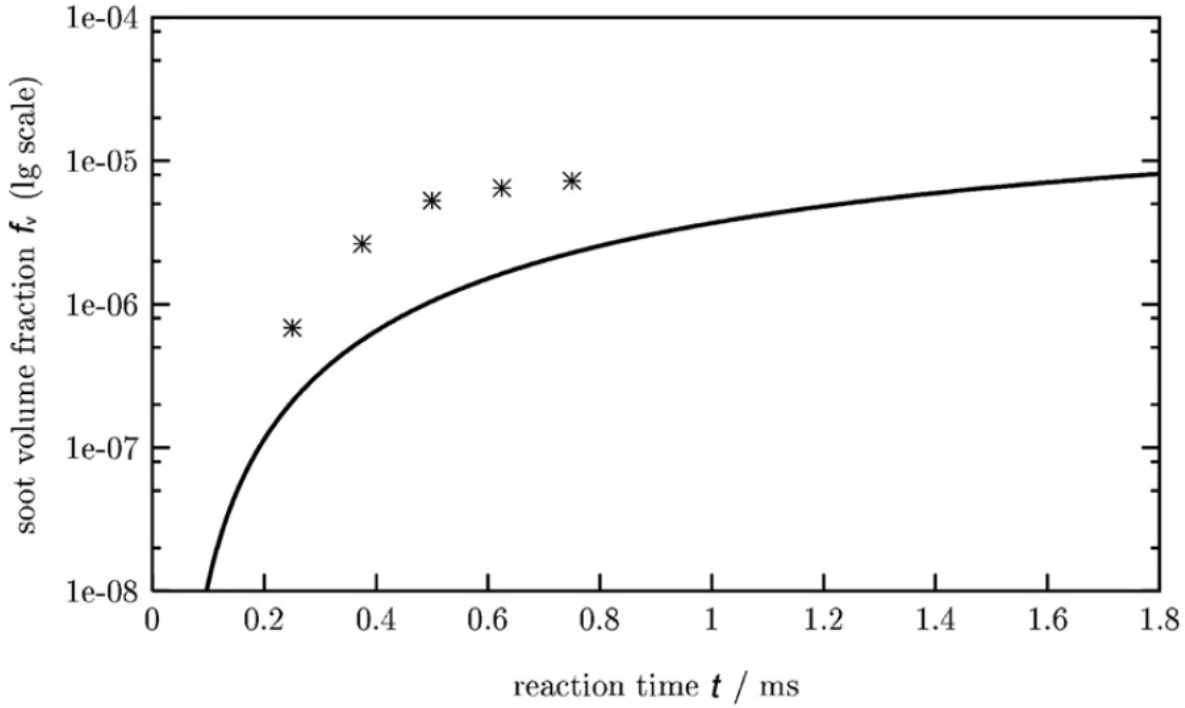

Fig. 2. Pyrolysis of benzene–argon mixture at initial conditions p = 5.4 MPa, T = 1721 K, $x(C_6H_6)$ = 0.002, and x(AR) = 0.998. Comparison with experimentally determined (symbols) [54] and calculated (curve) profiles [44] of the soot volume fraction fv (logarithmic scale) versus reaction time t .

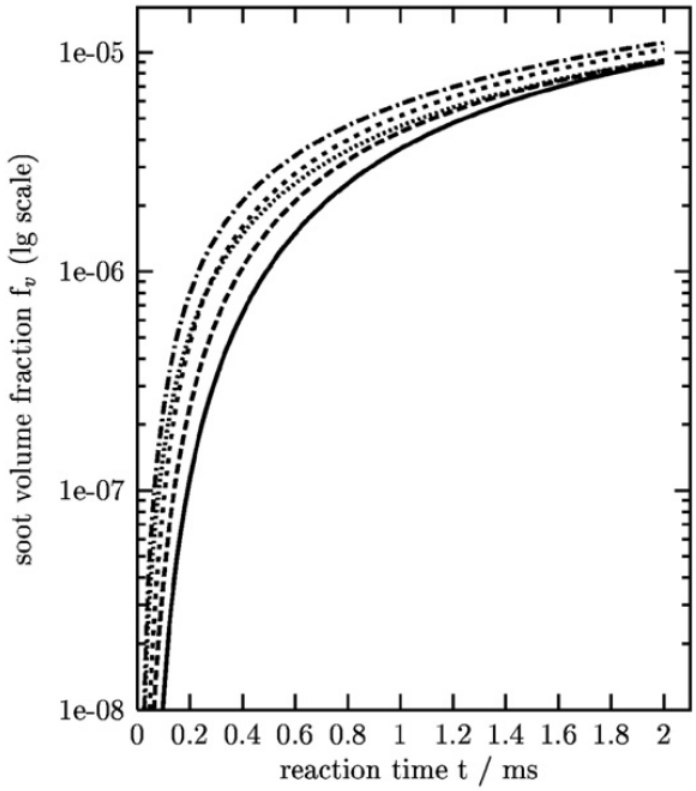

Fig. 3. Calculated soot volume fraction *fv* (logarithmic scale) for aliphatic–benzene–argon mixtures versus reaction time *t* at initial conditions p = 5.4 MPa, T = 1721 K, and mole fractions x(aliphatic) = 0.0002, $x(C_6H_6)$ = 0.0018, x(AR) = 0.998 (Mix2). Solid curve: 0.002 benzene; dash–dotted curve: 0.0018 benzene + 0.0002 MTBE; short dashed curve: 0.0018 benzene + 0.0002 i-C_4H_8; dotted curve: 0.0018 benzene + 0.0002 CH_3OH; dashed curve: 0.0018 benzene + 0.0002 C_2H_5OH.

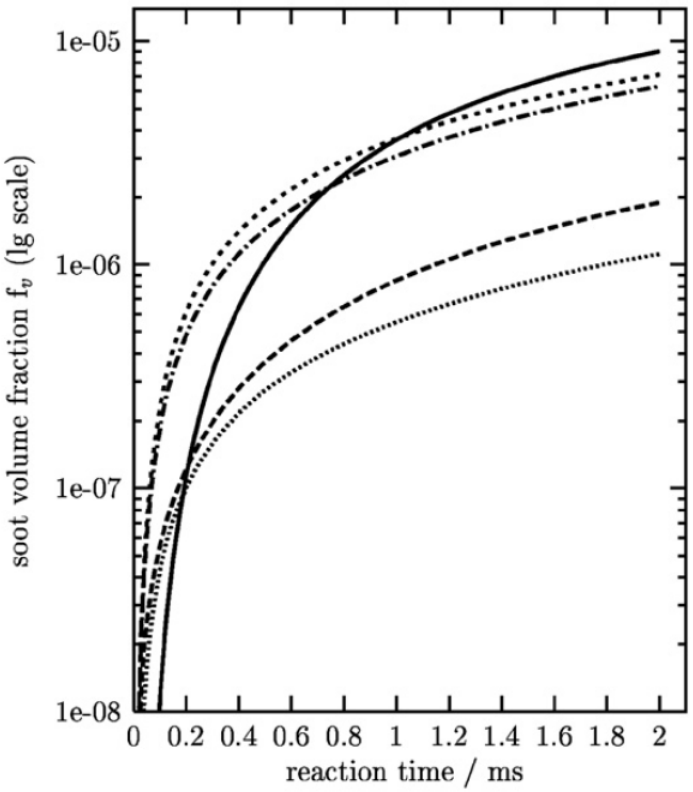

Fig. 4. Calculated soot volume fraction *fv* (logarithmic scale) for aliphatic–benzene–argon mixtures versus reaction time *t* at initial conditions *p* = 5.4 MPa, *T* = 1721 K, and mole fractions *x*(aliphatic) = 0.0014, *x*(C_6H_6) = 0.0006, *x*(AR) = 0.998 (Mix7). Solid curve: 0.002 benzene; dash–dotted curve: 0.0006 benzene + 0.0014 MTBE; short dashed curve: 0.0006 benzene + 0.0014 i-C_4H_8; dotted curve: 0.0006 benzene + 0.0014 CH_3OH; dashed curve: 0.0006 benzene + 0.0014 C_2H_5OH.

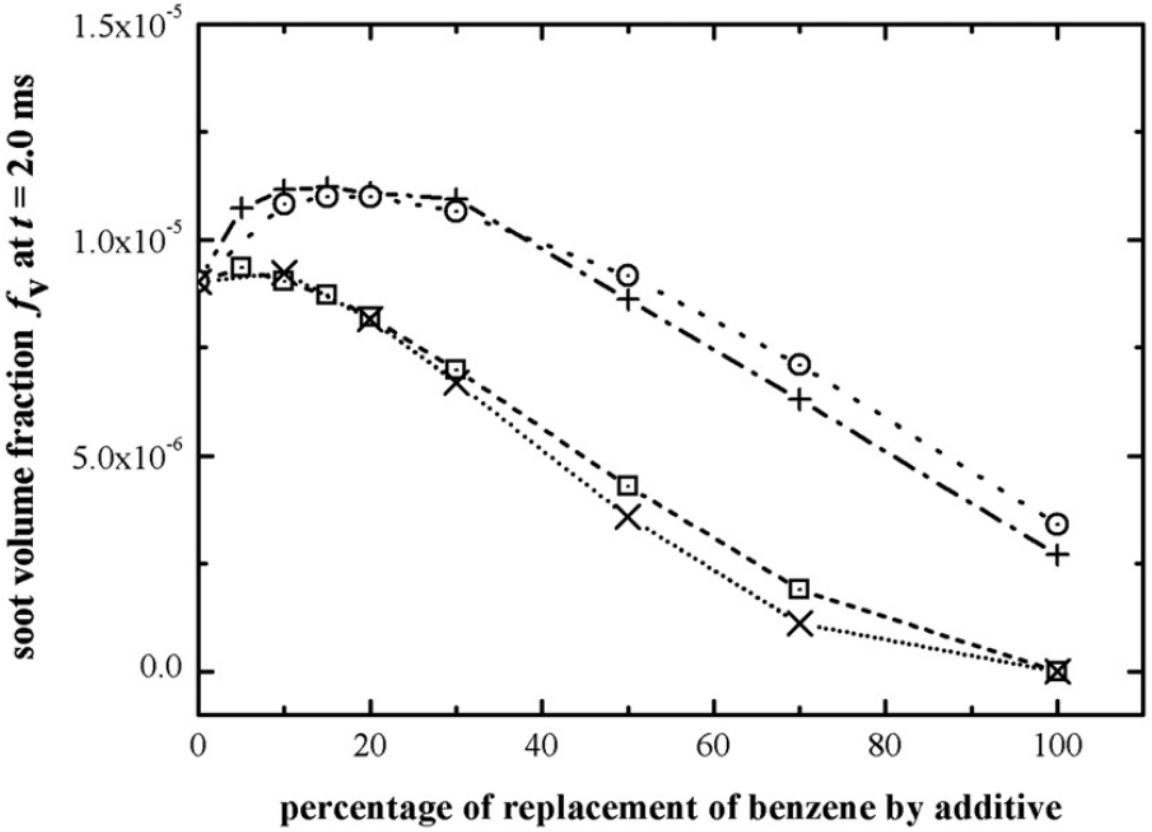

Fig. 5. Calculated soot volume fraction *f*v for aliphatic–benzene–argon mixtures at reaction time t = 2 ms versus percentage of benzene replaced by different additives, under initial conditions p = 5.4 MPa, T = 1721 K. Dash–dotted curve, plus: MTBE; short dashed curve, circle: i-C_4H_8; dotted curve, cross: CH_3OH; dashed curve, square: C_2H_5OH.

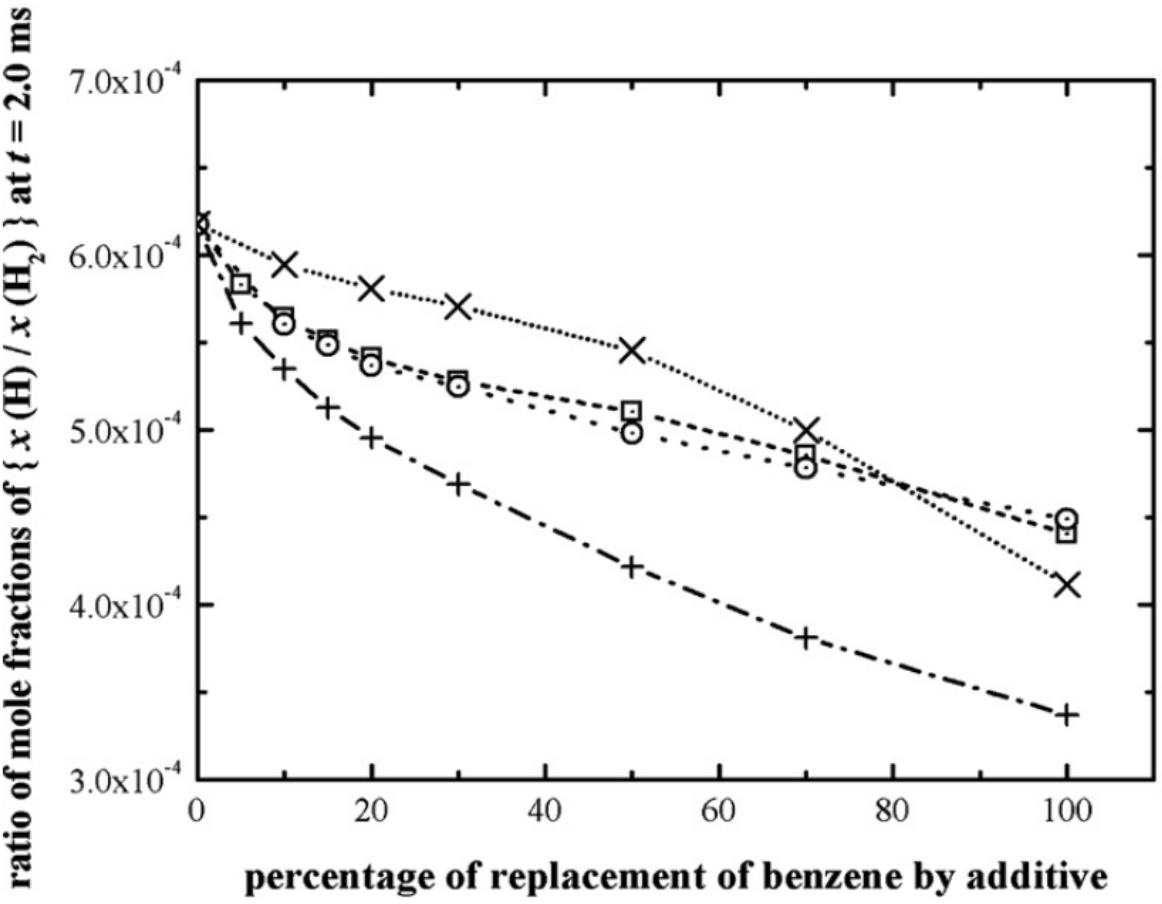

Fig. 6. Calculated ratio of mole fractions $\{x(H)/x(H_2)\}$ at reaction time t = 2 ms versus percentage of benzene replaced by different additives under initial conditions p = 5.4 MPa, T = 1721 K. Dash–dotted curve, plus: MTBE; short dashed curve, circle: i-C_4H_8; dotted curve, cross: CH_3OH; dashed curve, square: C_2H_5OH.

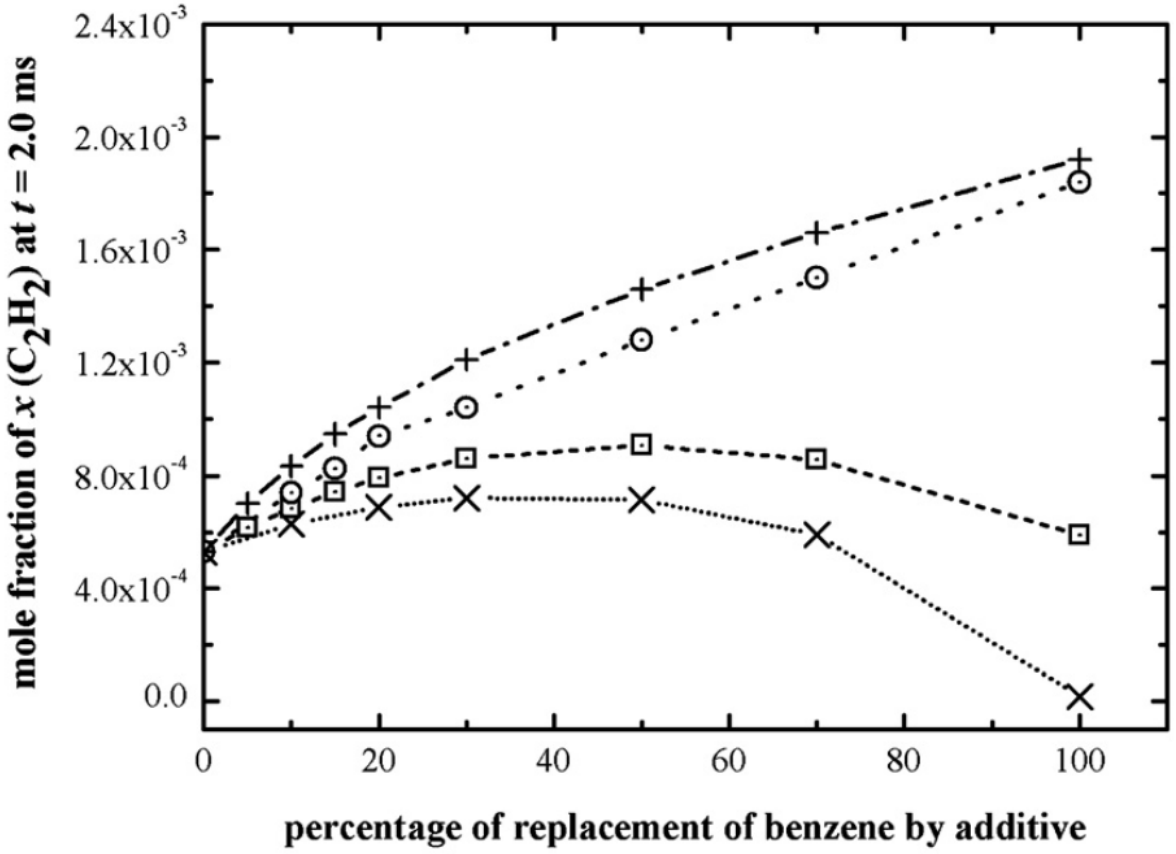

Fig. 7. Calculated mole fraction x of acetylene at the reaction time t = 2 ms versus percentage of benzene replaced by different additive; at the initial condition of p = 5.4 MPa, T = 1721 K. Dash–dotted curve, plus: MTBE; short dashed curve, circle: i-C_4H_8; dotted curve, cross: CH_3OH; dashed curve, square: C_2H_5OH.

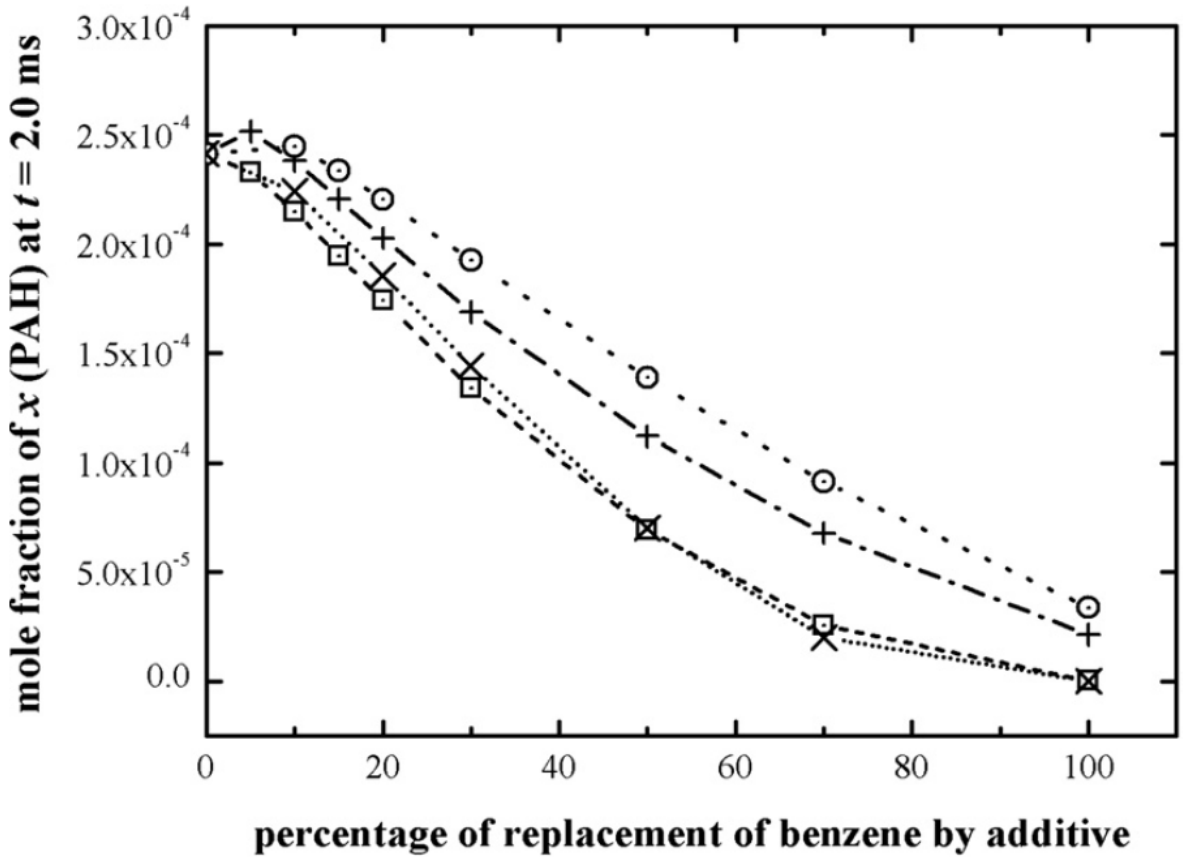

Fig. 8. Calculated sum of the mole fraction x of PAHs at the reaction time t = 2 ms versus percentage of benzene replaced by different aliphatics; at the initial condition of p = 5.4 MPa, T = 1721 K. Dash–dotted curve, plus: MTBE; short dashed curve, circle: i-C_4H_8; dotted curve, cross: CH_3OH; dashed curve, square: C_2H_5OH.

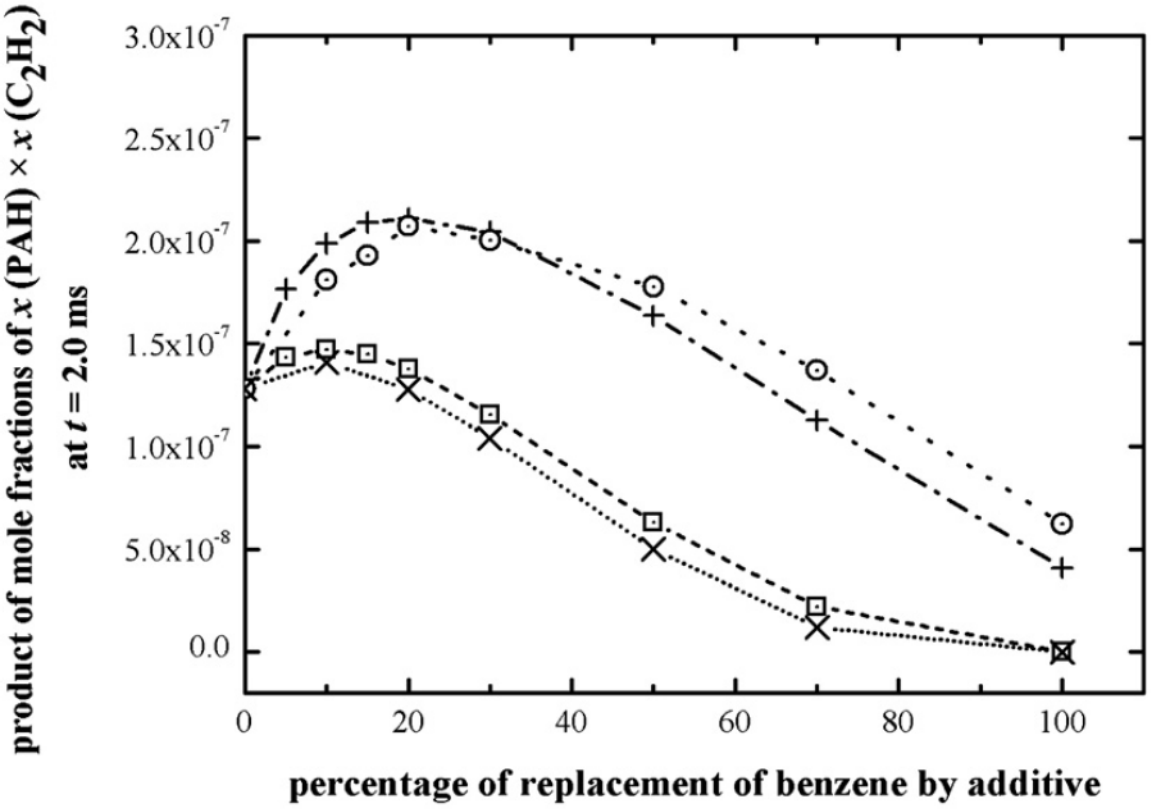

Fig. 9. Calculated mole fraction of x(PAHs) × $x(C_2H_2)$ at the reaction time t = 2 ms versus percentage of benzene replaced by different additives under initial conditions p = 5.4 MPa, T = 1721 K. Dash–dotted curve, plus: MTBE; short dashed curve, circle: i-C_4H_8; dotted curve, cross: CH_3OH; dashed curve, square: C_2H_5OH.

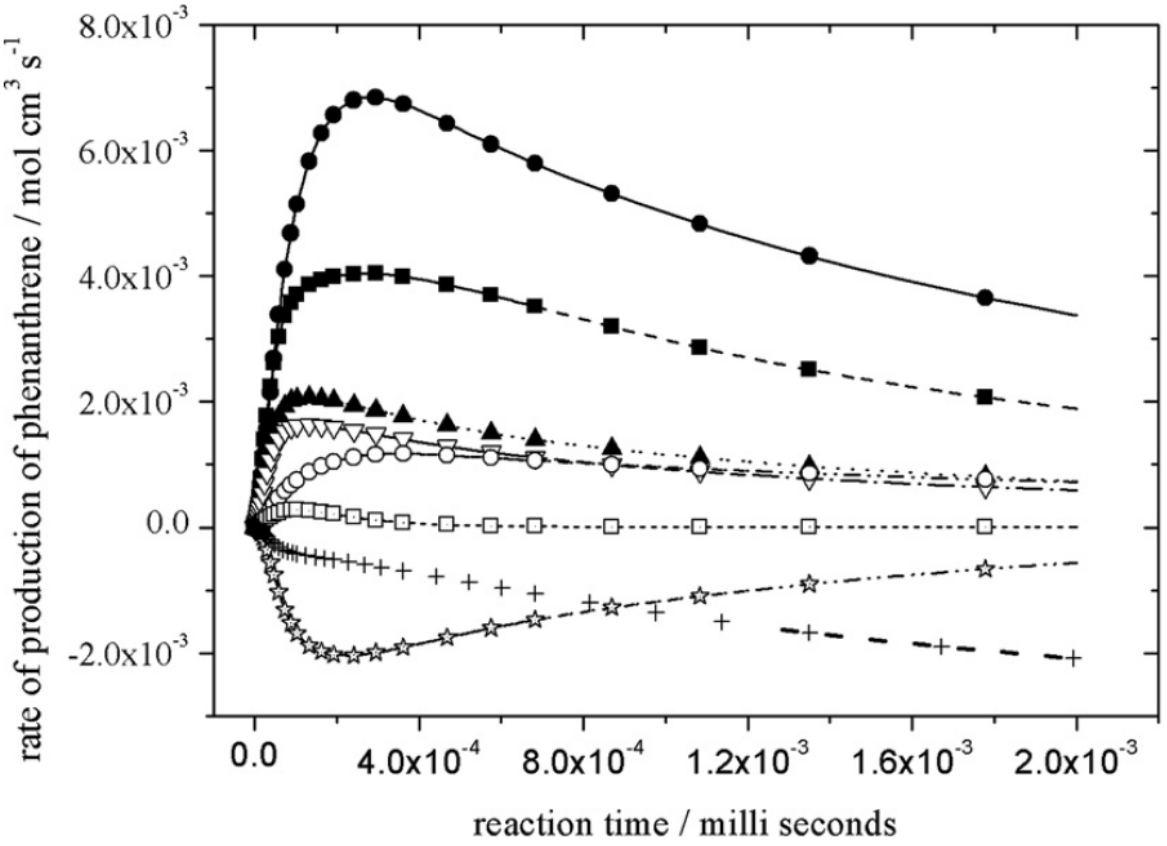

Fig. 10. Reaction flow analysis of MTBE–benzene–argon mixture (Mix7) for phenanthrene: filled circles: C_8H_6 + C_6H_5 → phenanthrene + H; filled squares: biphenyl + C_2H_2 →phenanthrene + H; filled triangles: $C_8H_5^*$ + C_6H_6 →phenanthrene + H; open triangles: $C_8H_5^-$ + C_6H_6 → phenanthrene + H; open squares: C_5H_5 + C_9H_7 → phenanthrene + 2H; open circles: stilbene→phenanthrene + H_2; pluses: phenanthrene + H→phenanthryl + H_2; stars: phenanthrene→anthracene.